GROWTH OF DAMAGE IN ADDITIVELY MANUFACTURED METAL-COMPOSITE JOINTS

P. N. Parkes[1], R. Butler[1]*, D. P. Almond[1]

[1]*Composites Research Unit, Department of Mechanical Engineering, University of Bath, Claverton Down, Bath, BA2 7AY, United Kingdom*
**R.Butler@bath.ac.uk*

Keywords: Ultrasound, Hybrid, Composite, Joints.

Abstract
The mechanical behaviour of a novel metallic-composite joining technology (HYPER) is investigated. Joints are strengthened with an array of pins built using additive layer manufacture. A new approach to pulse-echo ultrasonic evaluation was developed for this application in order to allow damage within joints to be monitored. It was found that the orientation of the specimen is critical due to the potential for the pins to scatter the incident ultrasonic wave. Damage was progressively induced within a batch of single lap HYPER coupons through repeated tensile loadings. The inspection methodology was successful at capturing the propagation of damage. It was found that the interface between adherends achieved a complete disbond without observable laminate damage or pin fracture. All pins then failed in an catastrophic manner due to excessive shear stress at their bases. Limit load was 21% higher than the ultimate load of a comparable unpinned joint. The ultimate load of the HYPER coupons was 650% higher than the same unpinned benchmark joint.

1 Introduction
Despite the increased use of carbon fibre reinforced plastics (CFRP) for primary aerospace structures, poor through-thickness strength and the low heat resistance of the resin matrix results in metals still being selected for a significant proportion of aircraft components. As a result, the use of both metallic and composite elements within aerospace structures will ultimately require them to be joined. At present, this is typically achieved using mechanical fasteners and adhesive bonding [1] which are inefficient approaches because of the increased weight of the fasteners and the number of manufacturing processes required; such as surface preparation. Hence, there is an urgent need to improve the manner in which these materials can be integrated. If their intrinsic properties can be advantageously exploited, it will allow structurally efficient and damage tolerant joints to be created. Hybrid Penetrative Reinforcement (HYPER) is one proposed solution to this challenge.

HYPER is a novel joining technology being developed by EADS Innovation Works [2]. Additive Layer Manufacturing (ALM) enables an array of pins to be sintered onto the surface of a titanium (Ti) adherend. The pins are then embedded into a CFRP adherend and co-cured, forming a combined mechanical interlock and adhesive bond. The pins and adhesive share applied loads more evenly than a bonded-bolted joint, reducing adhesive stress and delaying the onset of adhesive cracking. After the initiation of failure, the pins retard the propagation of the disbond which provides residual strength and increases ultimate load.

Currently, HYPER joining is at a low technology readiness level although work to date has shown impressive gains over comparable unpinned Ti-CFRP lap joints [3] and other similar technologies [4-7]. This is in part due to the unique pin profile.

Development work is ongoing in order to increase the maturity of HYPER and identify commercial applications. Research activities include refinement of the manufacturing processes as well as extensive mechanical testing and modelling to optimise the joint design. In addition, the capability to inspect HYPER joints during both manufacture and service will be essential (when implemented) and hence, a quality assurance regime is also being established.

This paper details two aspects of the joint development. Firstly, the selection of a suitable inspection methodology and secondly, the results of a mechanical test programme which subjected coupons to varying degrees of damage in order to characterise joint failure.

2 Non-Destructive Inspection Method

The design of HYPER joints makes them inherently challenging to inspect. The pins are approximately 1mm in diameter, conically headed (to aid embedding) and have a rough surface to improve adhesion with the resin matrix. Furthermore, they only penetrate partway through the laminate.

Graham et al. [6] have used a similar additive-pinning approach to join glass fibre and steel adherends in a double lap configuration and defects/damage could be observed visually through the transparent laminate. In this paper, HYPER joints between titanium and CFRP laminates are tested using a single lap construction (Figure 1) so an alternative method of inspection was required.

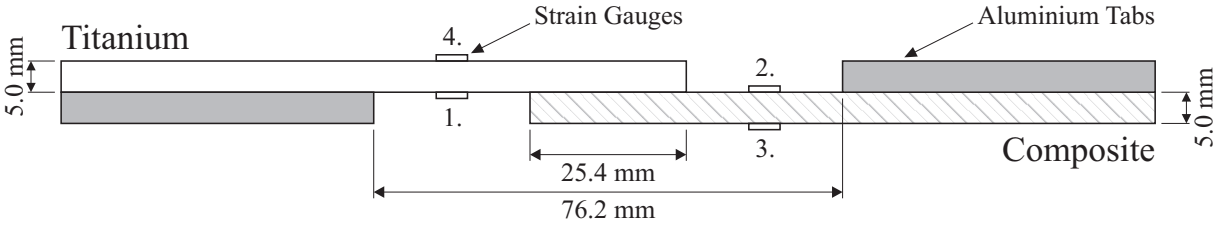

Figure 1. Assembly of single lap HYPER joint test coupons and identification of strain gauges 1-4.

It was not possible to image the adherend interface or pins using passive thermography due to inadequate spatial resolution given the thickness of the laminate and the size/depth of the pins. Ultrasonically stimulated thermography [8] could identify edge cracking around the overlap but offers no information regarding the integrity of the pins or bondline away from these boundaries. Whilst this could be used as a primary method of evaluation, a more comprehensive protocol would still be required.

Immersion pulse-echo ultrasound is a widely used for inspection of adhesive bondlines [9]. It has been found that the success of this technique, when applied to HYPER joining, varies depending on the orientation of the specimen. Assessment of the Ti-CFRP interface through the carbon side proved difficult as C-Scans were distorted by undesirable signal noise. It is believed that this was caused by the pins scattering the incident signal due to the angle and surface irregularity of the head feature. However, it has been found that inspection of the interface can be achieved from the metallic side due to the undistorted response of titanium.

ALM produces pins that are fused to (and an integral part of) the metallic adherend. Hence, when the ultrasonic probe passes over an unbroken pin, there is no discontinuity and the wave front travels into the pin; Figure 2(a-b). This is subsequently scattered so there is no signal reflected from the interface and as a result, the pin locations can be observed; shown in Figure 3. It can be also seen in Figure 3 that there is a reduction in signal along the upper, lower and right edges of the coupon interface. This is due to a loss of focus as the probe approaches the periphery of the specimen; Figure 2(c-e).

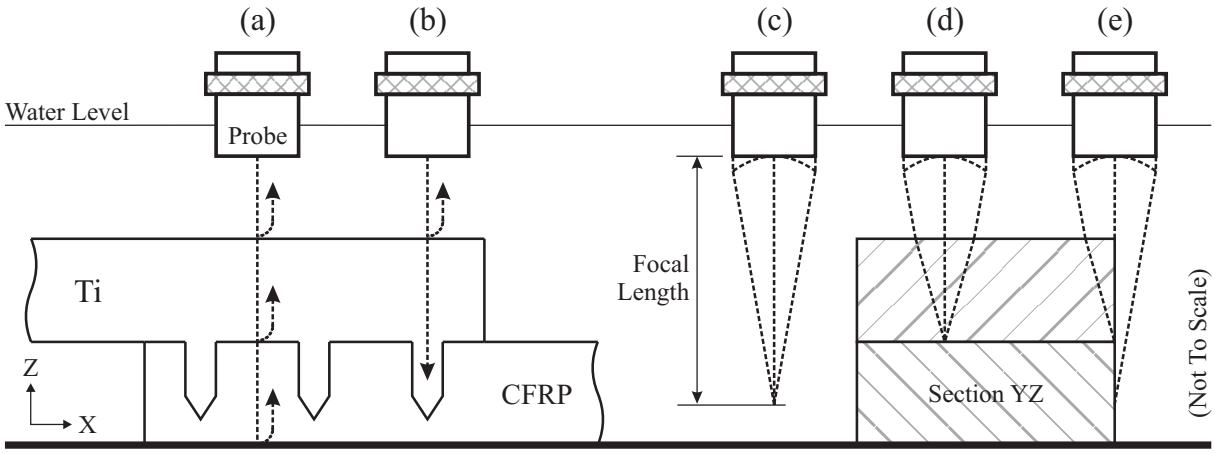

Figure 2. Pulse-echo ultrasonic inspection of adherend interface; (a) within overlap but away from pins signal is reflected from interface, (b) interface signal is lost over pins, (c) focal length of probe in water, (d) refraction reduces focal length in material, (e) coupon edge results in partial loss of focus.

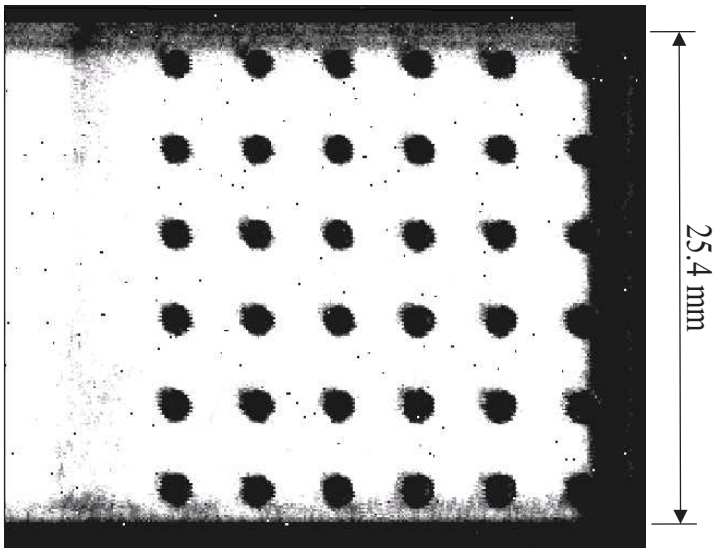

Figure 3. C-Scan image of adherend interface and pin locations. Intensity of white proportional to reflected signal strength. Threshold is low so no distinction can be made between good bonding and damage.

The system used to conduct the non-destructive testing was an Ultrasonic Sciences Limited, USL immersion C-Scan system with an Olympus Panametrics 35 MHz PVDF spherically focused probe. This polymer transducer was chosen as it offers an optimal impedance match to water and the high frequency provides excellent spatial resolution. The probe was offset from the coupon surface in order to focus incident sound waves onto the adherend interface; Figure 2d. Specimens were then raster scanned in the XY plane.

The integrity of interface bonding can also be established as differences in acoustic impedance cause variation in reflected signal energy - as described by Halmshaw [9]:

$$E_R = \left(\frac{Z_1 - Z_2}{Z_1 + Z_2} \right)^2 \qquad \text{where} \qquad Z_i = \rho_i \cdot c_i \tag{1}$$

and where E_R = proportion of incident wave energy reflected, Z = material acoustic impedance, ρ = material density, c = speed of sound in material, i = 1-2.

Material	**Density (kg/m^3)**	**Speed of Sound (m/s)**	**Impedance (Ns/m^3)**	**Proportion of Energy Reflected**
Titanium (Ti-6Al-4V)	4420	6100	26.962×10^6	N/A
CFRP (M21-T800S)	1580	3000	4.740×10^6	0.491
Water	998	1498	1.495×10^6	0.801
Air	1.2	343	412	0.999

Table 1. Properties of associated materials at 20˚C [10,11]. Values of reflected signal energy are for interfaces between titanium and the other materials listed, i.e. $Z_1 = 26.962 \times 10^6$ Ns/m^3.

It is assumed that a disbond will result in a thin layer of air between the titanium and CFRP adherends whereas in a region of good bonding, there would still be Ti-CFRP contact. Thus, a good bond will generate a weaker signal response than contact between either Ti-Air or Ti-Water (Table 1). If the C-Scan signal threshold is increased, the weaker signals from regions of good bonding can be removed so that disbonded areas can be distinguished. An example is shown in Figure 4.

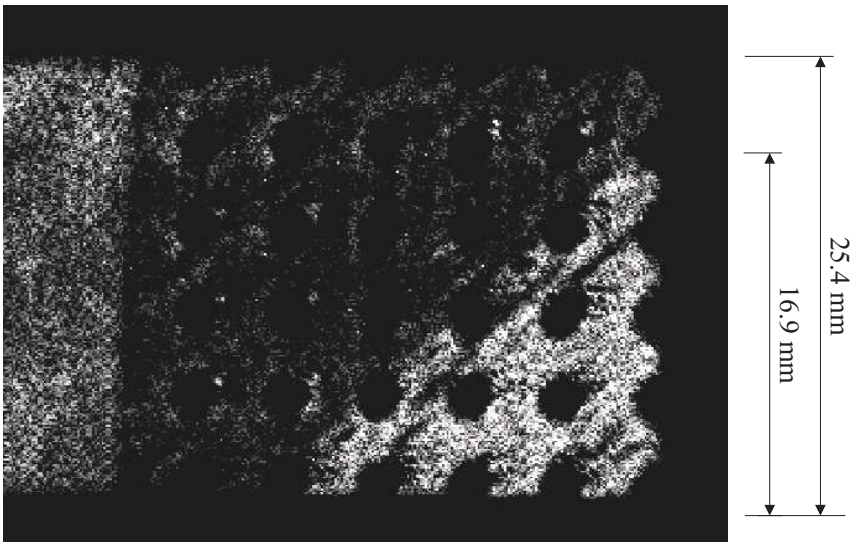

Figure 4. C-Scan with increased signal threshold to remove weaker signals from areas of good bonding. This reveals the Ti-Water interface (beyond the left edge of the overlap) and a disbond in the bottom-right corner.

3 Application of Inspection Method to Mechanical Test Programme

An extensive test programme is being undertaken to determine the mechanical performance of HYPER joints in order to optimise the pin design and provide experimental data to validate concurrent modelling activities. This work also includes characterisation of joint failure and in particular, interaction of adherend disbonding and pin fracture. This aspect of the campaign is described herein.

A series of HYPER lap shear coupons were loaded in tension until the initiation of failure and/or propagation of damage. This was observed visually during tests as a change in compliance or discontinuity on a load-strain plot or audibly when there was cracking. The test was then manually stopped, the coupon removed from the test machine and subjected to ultrasonic inspection (as described in Section 2) to determine the nature and magnitude of the damage. The coupon was then loaded again, but to a higher load, to establish the next failure event. This process was repeated until ultimate failure was achieved.

The test coupons conformed to ASTM D5868 [12] as shown in Figure 1. Each adherend was 101.2mm long, 25.4mm wide and nominally 5.0mm thick. The composite adherend was constructed using M21-T800 and a 20-ply quasi-isotropic layup: $[\pm 45/0/90/\pm 45/0/90/\pm 45]_S$. The gauge length was 76.2mm and the overlap 25.4mm - within which a uniformly distributed array of 36 ALM pins was built. Aluminium tabs were adhered (using Araldite 403) to maintain the adherend offset whilst allowing the coupon to be clamped in a set of coincident jaws and the load applied through the centreline of the specimen.

The test machine used was an Instron 5585 with displacement control set at a rate of 0.04mm/min. This rate was contrary to ASTM D5868 which specifies 13mm/min however this reduced velocity allowed subtle changes in coupon compliance to be observed and the test then stopped accordingly. Back-to-back strain gauges (SG1-4) were applied to each adherend (identified in Figures 1 and 5) and a Limess stereo Digital Image Correlation system was also used.

4 Results and Discussion

4.1 Effects of Experimental Setup

Before each test, prior to any load being applied, a small level of pre-strain was induced on the coupons due to tightening of the Instron jaws. A load-strain plot showed divergence of back-to-back strain gauge pairs indicating adherend curvature. This was caused by closure of the second jaw and displacement of the free end of the coupon in order to align and clamp it. This joint eccentricity was created during cure as the materials have different coefficients of thermal expansion [13]. Furthermore, due to rotational backlash in the mounting between the jaws and machine, it is thought that the process of tightening the jaws also induced twist about the load axis. Additional investigation is required to quantify the effects of this rotation on the performance of the joint.

4.2 Mechanical Behaviour

In total, three coupons were subjected to the testing procedure. Figure 5 shows the mechanical response of a typical coupon (ID13) during the first loading. A discontinuity was observed at 5.8 kN and the test was then stopped at 6.5 kN. This first failure event (F1) is thought to be the onset of adhesive cracking at the joint edge adjacent to SG2. Shear stress is highest at this side of the overlap due to the difference in adherend compliance [13].

This value of F1 is 21% higher than the ultimate load of a comparable unpinned Ti-CFRP joint [3] and hence, it can be assumed that HYPER pins delay the initiation of adhesive cracking. This is contrary to other hybrid joining schemes, where bolts (for example) have no influence on adhesive stresses at the edges of joints because of the minimum edge offsets that are specified by established design rules [1,14].

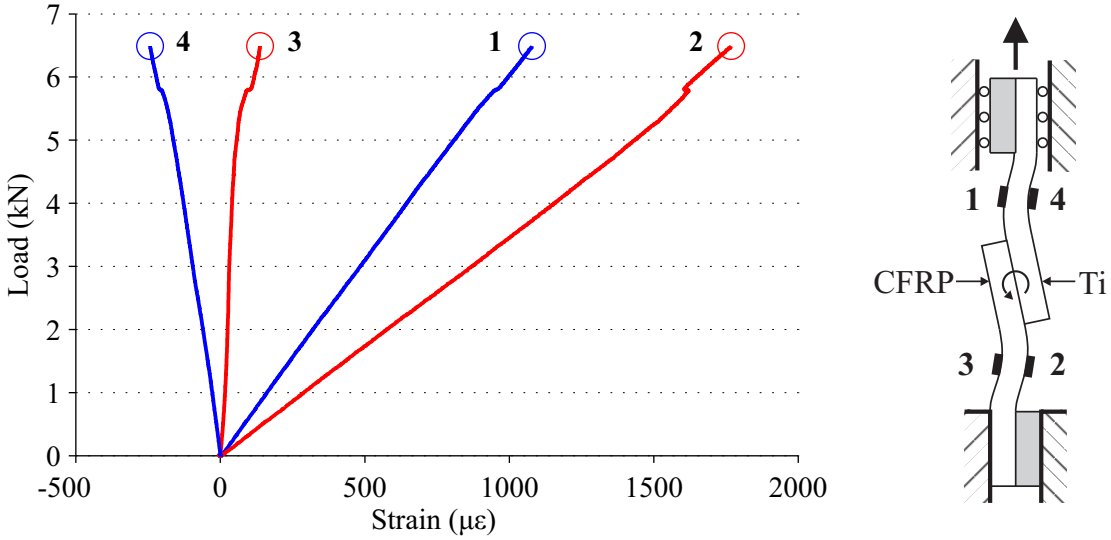

Figure 5. Recorded strains from gauges 1-4 for the first loading of coupon ID13.
Typical coupon rotation and mode shape also shown with identification of strain gauges (not to scale).

Coupon ID13 was loaded a total of six times before ultimate load was achieved. Figure 6 shows comparison of the loads/strains for each of these loadings. It can be seen that there was good correlation between consecutive loadings and variation resulting from the repeated setup procedure is considered to be negligible.

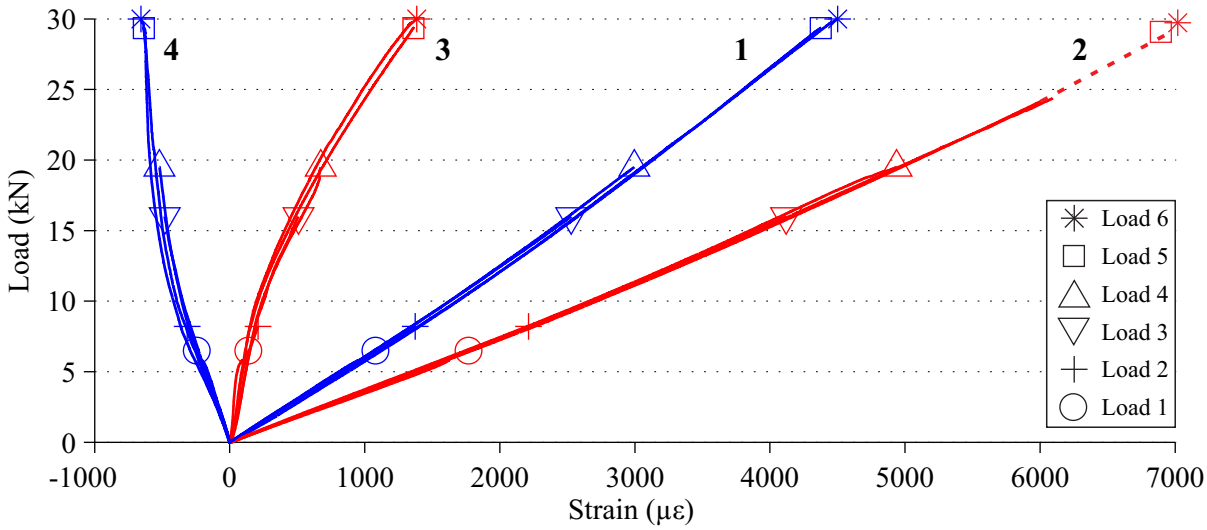

Figure 6. Recorded strains from gauges 1-4 for the six loadings of coupon ID13. Maximum force/strain for each loading shown with an individual marker. Dashed line shows extrapolation due to failure of SG2.

The non-linearity seen in Figure 6 was the result of the offset load path. This offset caused rotation of the overlap and subsequently, curvature was induced in the adherends - as depicted in Figure 5. This resulted in divergence of strain gauges 1+4 (Ti) and 2+3 (CFRP).

The rate of joint rotation was initially high but as the coupon approached an "optimum" mode shape (that best transmitted the applied load) this rate decayed exponentially [13]. Consequently, the rate at which the strain gauges diverged also decreased; as shown above.

It is thought that pin yielding had negligible effect on the response as the average adherend strains both showed a linear response and excellent correlation with the theoretical strains for the same load range.

4.2 Identification of Damage Growth

Through the use of the ultrasonic inspection technique described in Section 2, the propagation of damage at the adherend interface has been captured and is shown in Figure 7. It can be seen that there was only minimal damage following the first loading but that damage was then prominent on both sides of the overlap following the second loading; Figures 7b and 7c. However, it must be noted that due to the loss of transducer focus at the edge of the coupon, it was not possible to observe the region between the right-hand-most row of pins and the edge of the overlap. Therefore, damage may have been more extensive than is shown in Figure 7b.

As already stated, the difference in adherend stiffness results in higher shear stress the edge of the overlap adjacent to SG2. It would have been expected that damage would not only initiate at this side but would then continue to propagate from the same side as this boundary should remain more highly stressed regardless of disbond propagation. It is believed that the disbond initiated at the second side (adjacent to SG1) due to the pins sharing interface load, minimising peel/shear stress and temporarily preventing further growth from the first edge.

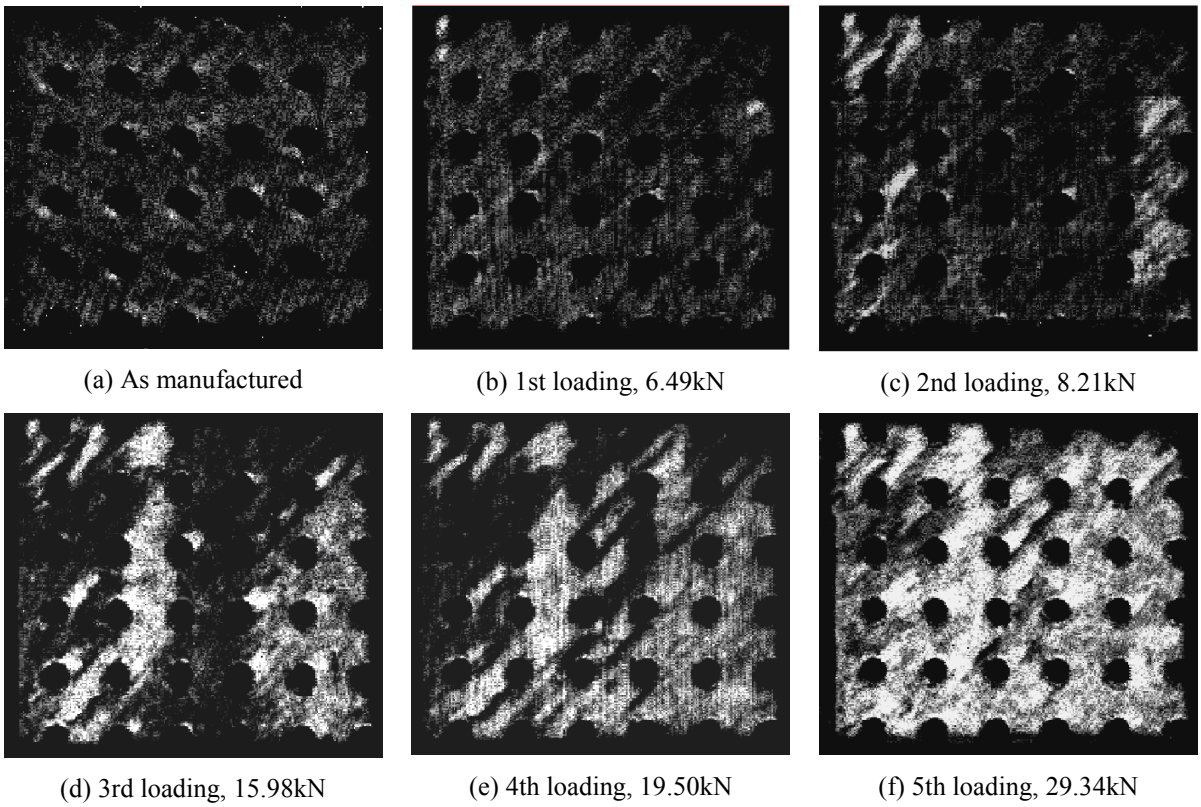

(a) As manufactured (b) 1st loading, 6.49kN (c) 2nd loading, 8.21kN

(d) 3rd loading, 15.98kN (e) 4th loading, 19.50kN (f) 5th loading, 29.34kN

Figure 7. C-Scans showing increasing levels of damage in the bondline of coupon ID13. Intensity of white regions signifies increased signal strength due to damage. Loads stated are maximum applied for that test.

After initiation has occurred at both edges, growth then occurs self-similarly but it can be seen that the extent of propagation is restricted by discrete amounts due to the pins; Figure 7d. The two sides of the disbond connect in Figure 7e and the interface then completely disbonds (Figure 7f). It should be noted that none of the pins have fractured at this stage. The ultimate load of the coupons was limited by the shear strength of the pins - no laminate damage was seen. Catastrophic failure was instantaneous (within 0.004 seconds) rather than a progressive row-by-row "domino" effect. The average maximum load was 31.0 kN which equates to an applied stress of 248.1 MPa and was 6.5 times the magnitude of the benchmark joint.

5 Conclusions

A non-destructive, ultrasonic inspection technique for HYPER has been established and validated during a series of mechanical tests. The condition of the joint interface can be assessed by inspection of the specimen through the metallic adherend and adjustment of the C-Scan signal threshold.

This approach could be limited by access restrictions in a commercial application and if the geometry of metallic adherend was not uniform. Focusing of the transducer near the coupon edge also prevented accurate quantification of the damage at F1 (limit load). Despite this restriction, the test objectives were met and the progressive growth of damage was observed within the tested coupons.

An interface disbond initiated at the edge adjacent to the more compliant adherend but then propagated self-similarly from opposing boundaries as the pins helped to reduce the peak peel/shear stress. The interface disbond penetrates the overlap entirely before any pin damage occurs. Final failure was instantaneous due to pin fracture at a load of 31.0 kN (248.1 MPa).

The work herein forms only a small part of the ongoing HYPER joint development programme. The influence of adherend thermal mismatch, fatigue and impact damage on joint performance are currently under investigation.

Acknowledgements

The authors would like to thank EADS Innovation Works UK for financial sponsorship of the project. In particular, Jonathan Meyer, André De Oliveira and Lewis Balfour for their guidance and practical assistance.

References

[1] Cheung C.H.E., Gray P.M., Mabson G.E., Lin K.Y. *Analysis of Fasteners as Disbond Arrest Mechanism for Laminated Composite Structures*. Proceedings of 51st AIAA/ ASME/ASCE/AHS/ASC, Orlando, USA (2010).
[2] Meyer J., Johns D. *Hybrid Component*. Patent, WO 2010/112904 A1 (2010).
[3] EADS Innovation Works. *Private communications* (2012).
[4] Tu W., Wen P.H., Hogg P.J., Guild F. *Optimisation of the protrusion geometry in Comeld joints*. Composites Science and Technology, **71**, pp.868-876 (2011).
[5] Ucsnik S., Scheerer M., Zaremba S., Pahr D.H. *Experimental investigation of a novel hybrid metal-composite joining technology*. Composites: Part A, **41**, pp.369–374 (2010).
[6] Graham D.P., Rezai A., Baker D., Smith P.A., Watts J.F. *A Hybrid Joining Scheme For High Strength Multi-Material Joints*. Proceedings of ICCM 18, Jeju Island, Korea (2011).
[7] Nogueira A.C., Drechsler K., Hombergsmeier E. *Analysis of the Static and Fatigue Strength of a Damage Tolerant 3D-Reinforced Joining Technology on Composite Single Lap Joints*. Proceedings of 53rd AIAA/ASME/ASCE/AHS/ASC, Hawaii, USA (2012).
[8] Favro L.D., Han X., Ouyang Z., Sun G., Sui H., Thomas R.L. *Infrared imaging of defects heated by a sonic pulse*. American Institute of Physics Rev. Sci. Instrum. **71**, pp.2418-2421 (2000).
[9] Halmshaw R. *Non-Destructive Testing*. Edward Arnold, London, UK, pp.106-187 (1991).
[10] Gale W.F., Totemeier T.C. *Smithells Metal Reference Book*. Elsevier Butterworth-Heinemann, Oxford, UK (2004).
[11] Hexcel. *HexPly M21 Product Data,* www.hexcel.com, accessed 21/03/2012 (2010).
[12] ASTM D5868-01. *Standard Test Method for Lap Shear Adhesion for Fiber Reinforced Plastic (FRP) Bonding* (2008).
[13] Hart-Smith L.J. *Adhesive bonded single lap joints*. NASA Report CR 112236 (1973).
[14] Imperiale V.A., Cosentino E., Weaver P.M., Bond I.P. *Compound joint: A novel design principle to improve strain allowables of FRP composite stringer run-outs*. Composites: Part A, **41**, pp.521-531 (2010).